Zero-Field Slow Magnetic Relaxation from Single Co(II) Ion: A Transition Metal Single-Molecule Magnet with High Anisotropy Barrier

Yuan-Yuan Zhu,[a,b] Chang Cui,[a] Yi-Quan Zhang,[a] Jun-Hua Jia,[a] Xiao Guo,[a] Chen Gao,[a] Kang Qian,[a] Shang-Da Jiang,[a] Bing-Wu Wang,*[a] Zhe-Ming Wang,[a] and Song Gao*[a]

[a]Beijing National Laboratory of Molecular Science, State Key Laboratory of Rare Earth Materials Chemistry and Applications, College of Chemistry and Molecular Engineering, Peking University, Beijing 100871, P. R. China.

[b]Key Laboratory of Advanced Functional Materials and Devices, Anhui Province, School of Chemical Engineering, Hefei University of Technology, Anhui, 230009, People's Republic of China.

To whom correspondence should be addressed. E-mail: gaosong@pku.edu.cn, wangbw@pku.edu.cn. Fax: (+86) 10-6275-1708.

Physical measurement

Magnetic measurements were performed on a Quantum Design MPMS XL-5 and PPMS-9T (EC-II) SQUID magnetometer on polycrystalline samples. Data were corrected for the diamagnetism of the samples using Pascal constants and of the sample holder by measurement. Dc magnetic susceptibility measurement up to 12 T was performed on Wuhan High Magnetic Field Center (WHMFC) with PPMS-16.

The X-ray measurements of **1** were carried on a Nonius KappaCCD diffractometer with Mo Kα radiation (λ = 0.71073 Å) at 200 K. Empirical absorption corrections were applied using the Sortav program. The structure was solved using SHELXS-97 program[1] and refined by a full matrix least squares technique based on F^2 using SHELXL 97 program.[2]

Experimental Section

Caution! Although not encountered in our experiments, perchlorate salts in the presence of organic ligands are potentially explosive. Only a small amount of the materials should be prepared and handled with care.

Synthesis

All starting materials were purchased as reagent grade and were used without further purification. The synthesis procedure of the Schiff base ligands are described as below.

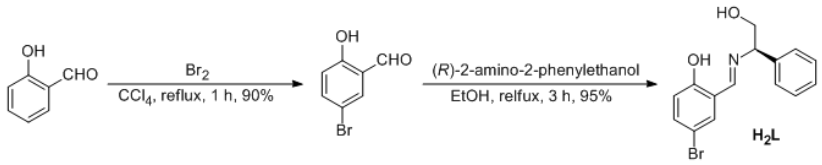

Scheme S1. The synthesis route of ligand H_2L.

Compound 5-bromo-2-hydroxybenzaldehyde was synthesizd according to the literature method.[3] ^{1}H NMR (400 MHz, $CDCl_3$): δ 10.93 (s, 1 H), 9.84 (s, H), 7.68 (d, J = 2.4 Hz, 1 H), 7.60 (d d, J_1 = 8.8 Hz, J_2 = 2.4 Hz, 1 H), 6.91 (d, J = 8.8 Hz).

Compound H_2L. A solution of 5-bromo-2-hydroxybenzaldehyde (2.01 g, 10.0 mmol) and (*R*)-2-amino-2-phenylethanol (1.37 g, 10.0 mmol) in ethanol was stirred under reflux for 3 h and the color of the solution was turned to yellow. After removal of the solvents under reduced pressure, the crude product was purified by recrystallization in the mixture solvent of ethanol and petroleum ether to give compound **H_2L** as needlelike crystals (3.04 g, 95 %). ^{1}H NMR (400 MHz, $CDCl_3$): δ 13.30 (br, 1 H), 8.40 (s, 1 H), 7.41–7.29 (m, 7 H), 6.87 (d, J = 8.4 Hz, 1 H), 4.48 (t, J = 6.4 Hz, 1 H), 3.93 (d, J = 6.4 Hz, 2 H). Anal. Calcd for $C_{15}H_{14}BrNO_2$: C, 56.27; H, 4.41; N, 4.37. Found: C, 56.13; H, 4.35; N, 4.35. MS (ESI): m/z 320.08 $[M + 1]^+$. IR (pure sample): ν = 3480(m), 3417(m), 3085(w), 3060(w), 3028(w), 3004(w), 2983(w), 2969(w), 2923(w), 2882(w), 2865(w), 2743(w), 2682(w), 1952(w), 1881(w), 1831(w), 1812(w), 1770(w), 1698(w), 1630(s), 1570(m), 1476(s), 1454(m), 1374(m), 1340(w), 1313(w), 1280(s), 1222(w), 1207(m), 1184(m), 1130(w), 1078(m), 1057(m), 1033(m), 1028(m), 1000(w), 985(w), 974(w), 948(w), 915(m), 894(m), 854(w), 825(s), 810(m), 778(w), 764(m), 734(w), 699(m), 681(w), 640(w), 626(w).

Synthesis of $(HNEt_3)^+[Co^{II}Co^{III}_3(L)_6]^-$, 1. A mixture of H_2L (480 mg, 1.5 mmol) and Et_3N (4.3 mL, 3 mmol) in methanol (20.0 mL) was stirred at room temperature. A dark brown precipitate was generated as soon as the solution of $Co(ClO_4)_2 \cdot 6H_2O$ (366 mg, 1 mmol) in methanol (10.0 mL) was added dropwise, and the mixture was stirred at room temperature for 12 h. The resulting solution was filtered and the solvent was removed under vacuum. The dark brown precipitate obtained was dried under vacuum then redissoved in hot DMF (40.0 mL). Dark red block crystals were obtained within two weeks in 50-60% yield by slow evaporation of the resulting solution. The crystals are stable at room temperature and no loss of solvent is observed. Anal. Calcd for $C_{96}H_{88}Br_6Co_4N_7O_{12} \cdot 5DMF \cdot 2H_2O$: C, 50.34; H, 4.83; N, 6.35. Found: C, 50.42; H, 4.73; N, 6.66. IR (pure sample): ν = 3647(w), 3060(w), 3028(w), 2920(w), 2857(w), 2694(w), 1890(w), 1668(m), 1637(s), 1590(m), 1521(m), 1494(w), 1461(s), 1420(m), 1373(m), 1331(w), 1315(m), 1247(w), 1196(w), 1174(m), 1135(w), 1092(w), 1065(w), 1030(m), 963(w), 947(w), 909(w), 870(w), 821(m), 763(w), 731(w), 706(w), 691(w), 653(m), 611(w). HRMS (ESI-MS): Calcd. For $C_{96}H_{89}Br_6Co_4N_7O_{12}^+$: 2246.89361, Found: 2246.86759 (cation mode).

Crystal data for **1**: $C_{110.10}H_{109}Br_6Co_4N_{11.70}O_{17.50}$, Mr = 2539.30, Orthorhombic, $P2_12_12_1$, a = 12.6611(1), b = 19.0777(1), c = 47.5848(4) Å, α = 90, β = 90, γ = 90°, V = 11493.9(2) Å^3, Z = 4, T = 200(2) K, GOF = 0.971, Flack parameters: 0.014(6), R1(final) = 0.0450, $wR2$ = 0.1078. CCDC 881924.

Table S1. Selected bond lengths (Å) and angles (°) for **1**.

Co(1)-O(2)	2.135(4)	Co(1)-O(4)	2.154(4)
Co(1)-O(6)	2.121(4)	Co(1)-O(8)	2.168(4)
Co(1)-O(10)	2.171(4)	Co(1)-O(12)	2.087(4)
Co(2)-O(1)	1.896(4)	Co(2)-O(2)	1.900(4)
Co(2)-O(3)	1.887(4)	Co(2)-O(4)	1.899(4)
Co(2)-N(1)	1.901(4)	Co(2)-N(2)	1.914(5)
Co(3)-O(5)	1.898(4)	Co(3)-O(6)	1.887(4)
Co(3)-O(7)	1.890(4)	Co(3)-O(8)	1.902(4)
Co(3)-N(3)	1.906(5)	Co(3)-N(4)	1.886(5)
Co(4)-O(9)	1.883(4)	Co(4)-O(10)	1.901(4)
Co(4)-O(11)	1.900(4)	Co(4)-O(12)	1.908(4)
Co(4)-N(5)	1.902(5)	Co(4)-N(6)	1.900(5)

O(12)-Co(1)-O(6)	117.47(15)	O(12)-Co(1)-O(2)	144.56(14)
O(6)-Co(1)-O(2)	91.56(14)	O(6)-Co(1)-O(4)	143.56(14)
O(12)-Co(1)-O(4)	91.95(14)	O(12)-Co(1)-O(8)	89.24(14)
O(2)-Co(1)-O(4)	71.89(14)	O(2)-Co(1)-O(8)	120.80(14)
O(6)-Co(1)-O(8)	71.46(14)	O(12)-Co(1)-O(10)	72.28(14)
O(4)-Co(1)-O(8)	89.11(14)	O(2)-Co(1)-O(10)	88.83(14)
O(6)-Co(1)-O(10)	90.21(14)	O(8)-Co(1)-O(10)	144.54(14)
O(4)-Co(1)-O(10)	120.67(14)	O(3)-Co(2)-O(1)	90.34(18)
O(3)-Co(2)-O(4)	176.24(17)	O(1)-Co(2)-O(4)	93.41(16)
O(3)-Co(2)-O(2)	93.23(16)	O(1)-Co(2)-O(2)	175.86(17)
O(4)-Co(2)-O(2)	83.03(16)	O(3)-Co(2)-N(1)	85.38(18)
O(1)-Co(2)-N(1)	94.07(18)	O(4)-Co(2)-N(1)	94.62(18)
O(2)-Co(2)-N(1)	84.14(18)	O(3)-Co(2)-N(2)	94.62(19)
O(1)-Co(2)-N(2)	86.25(18)	O(4)-Co(2)-N(2)	85.35(18)
O(2)-Co(2)-N(2)	95.54(18)	N(1)-Co(2)-N(2)	179.7(2)
N(4)-Co(3)-O(7)	94.69(19)	O(6)-Co(3)-O(7)	93.97(17)
N(4)-Co(3)-O(5)	85.63(19)	O(6)-Co(3)-O(5)	175.21(18)
O(7)-Co(3)-O(5)	90.78(18)	N(4)-Co(3)-O(8)	84.16(18)
O(6)-Co(3)-O(8)	82.76(16)	O(7)-Co(3)-O(8)	176.42(18)
O(5)-Co(3)-O(8)	92.50(16)	N(4)-Co(3)-N(3)	178.9(2)
O(6)-Co(3)-N(3)	84.76(18)	O(7)-Co(3)-N(3)	84.49(19)
O(5)-Co(3)-N(3)	95.11(18)	O(8)-Co(3)-N(3)	96.62(18)
N(4)-Co(3)-O(6)	94.58(19)	N(5)-Co(4)-O(12)	96.54(18)
O(9)-Co(4)-N(6)	86.50(18)	O(9)-Co(4)-O(11)	90.85(18)
N(6)-Co(4)-O(11)	94.17(18)	O(9)-Co(4)-O(10)	174.98(17)
N(6)-Co(4)-O(10)	93.96(18)	O(11)-Co(4)-O(10)	94.10(17)
O(9)-Co(4)-N(5)	94.51(19)	N(6)-Co(4)-N(5)	178.7(2)
O(11)-Co(4)-N(5)	85.02(18)	O(10)-Co(4)-N(5)	85.10(18)
O(9)-Co(4)-O(12)	92.55(17)	N(6)-Co(4)-O(12)	84.20(17)
O(11)-Co(4)-O(12)	176.13(17)	O(10)-Co(4)-O(12)	82.52(16)

Table S2. The BVS calculation result using PLATON software.[4,5]

Co1:

Bond Valence Analysis - Assume Valence = 2 -- Min. BondVal Contribution = 0.04 * Cation Val.

Nr	Bond		Dist	R	B	BVal	Sum	Diff
1	Co1	O12	2.0941	1.6920	0.37	0.337	0.337	1.663
2	Co1	O6	2.1231	1.6920	0.37	0.312	0.649	1.351
3	Co1	O2	2.1351	1.6920	0.37	0.302	0.951	1.049
4	Co1	O4	2.1477	1.6920	0.37	0.292	1.243	0.757
5	Co1	O8	2.1641	1.6920	0.37	0.279	1.522	0.478
6	Co1	O10	2.1708	1.6920	0.37	0.274	**1.796**	**0.204**

Bond Valence Analysis - Assume Valence = 3 -- Min. BondVal Contribution = 0.04 * Cation Val.

Nr	Bond		Dist	R	B	BVal	Sum	Diff
1	Co1	O12	2.0941	1.6370	0.37	0.291	0.291	2.709
2	Co1	O6	2.1231	1.6370	0.37	0.269	0.560	2.440
3	Co1	O2	2.1351	1.6370	0.37	0.260	0.820	2.180
4	Co1	O4	2.1477	1.6370	0.37	0.252	1.071	1.929
5	Co1	O8	2.1641	1.6370	0.37	0.241	1.312	1.688
6	Co1	O10	2.1708	1.6370	0.37	0.236	1.548	1.452

Co2:

Bond Valence Analysis - Assume Valence = 2 -- Min. BondVal Contribution = 0.04 * Cation Val.

Nr	Bond		Dist	R	B	BVal	Sum	Diff
1	Co2	O3	1.8924	1.6920	0.37	0.582	0.582	1.418
2	Co2	O1	1.8933	1.6920	0.37	0.580	1.162	0.838
3	Co2	O4	1.9005	1.6920	0.37	0.569	1.731	0.269
4	Co2	O2	1.9005	1.6920	0.37	0.569	2.301	0.301
5	Co2	N1	1.9053	1.6500	0.37	0.502	2.802	0.802
6	Co2	N2	1.9114	1.6500	0.37	0.493	3.296	1.296

Bond Valence Analysis - Assume Valence = 3 -- Min. BondVal Contribution = 0.04 * Cation Val.

Nr	Bond		Dist	R	B	BVal	Sum	Diff
1	Co2	O3	1.8924	1.6370	0.37	0.501	0.501	2.499
2	Co2	O1	1.8933	1.6370	0.37	0.500	1.002	1.998
3	Co2	O4	1.9005	1.6370	0.37	0.491	1.492	1.508
4	Co2	O2	1.9005	1.6370	0.37	0.491	1.983	1.017
5	Co2	N1	1.9053	1.7500	0.37	0.657	2.640	0.360
6	Co2	N2	1.9114	1.7500	0.37	0.646	**3.287**	**0.287**

Co3:

Bond Valence Analysis - Assume Valence = 2 -- Min. BondVal Contribution = 0.04 * Cation Val.

Nr	Bond		Dist	R	B	BVal	Sum	Diff
1	Co3	O6	1.8903	1.6920	0.37	0.585	0.585	1.415
2	Co3	N4	1.8951	1.6500	0.37	0.516	1.101	0.899
3	Co3	O7	1.8982	1.6920	0.37	0.573	1.673	0.327
4	Co3	O5	1.8990	1.6920	0.37	0.572	2.245	0.245
5	Co3	O8	1.8990	1.6920	0.37	0.571	2.816	0.816
6	Co3	N3	1.9034	1.6500	0.37	0.504	3.321	1.321

Bond Valence Analysis - Assume Valence = 3 -- Min. BondVal Contribution = 0.04 * Cation Val.

Nr	Bond		Dist	R	B	BVal	Sum	Diff
1	Co3	O6	1.8903	1.6370	0.37	0.504	0.504	2.496
2	Co3	N4	1.8951	1.7500	0.37	0.676	1.180	1.820
3	Co3	O7	1.8982	1.6370	0.37	0.494	1.673	1.327
4	Co3	O5	1.8990	1.6370	0.37	0.493	2.166	0.834
5	Co3	O8	1.8990	1.6370	0.37	0.493	2.659	0.341
6	Co3	N3	1.9034	1.7500	0.37	0.661	**3.319**	**0.319**

Co4:

Bond Valence Analysis - Assume Valence = 2 -- Min. BondVal Contribution = 0.04 * Cation Val.

Nr	Bond		Dist	R	B	BVal	Sum	Diff
1	Co4	O9	1.8854	1.6920	0.37	0.593	0.593	1.407
2	Co4	N6	1.8993	1.6500	0.37	0.510	1.103	0.897
3	Co4	O11	1.9001	1.6920	0.37	0.570	1.672	0.328
4	Co4	O10	1.9001	1.6920	0.37	0.570	2.242	0.242
5	Co4	O12	1.9041	1.6920	0.37	0.564	2.806	0.806
6	Co4	N5	1.9043	1.6500	0.37	0.503	3.309	1.309

Bond Valence Analysis - Assume Valence = 3 -- Min. BondVal Contribution = 0.04 * Cation Val.

Nr	Bond		Dist	R	B	BVal	Sum	Diff
1	Co4	O9	1.8854	1.6370	0.37	0.511	0.511	2.489
2	Co4	N6	1.8993	1.7500	0.37	0.668	1.179	1.821
3	Co4	O11	1.9001	1.6370	0.37	0.491	1.670	1.330
4	Co4	O10	1.9001	1.6370	0.37	0.491	2.161	0.839
5	Co4	O12	1.9041	1.6370	0.37	0.486	2.647	0.353
6	Co4	N5	1.9043	1.7500	0.37	0.659	**3.306**	**0.306**

Magnetic susceptibility data fitting

Three ligand field parameters B_{20}, B_{40} and B_{43} in Wybourne notation are needed for the description of central Co(II) ion in D_3 symmetry. These parameters obtained from magnetic susceptibility data fitting for **1** are $B_{20} = 4.416 \times 10^4$ cm^{-1}, $B_{40} = 3.479 \times 10^4$ cm^{-1}, $B_{43} = -1.342 \times 10^3$ cm^{-1}.

CASSCF calculations on model structure of individual molecule **1** have been carried out with MOLCAS

7.6 program package.[6] The influence of the diamagnetic Co(III) ions is simulated by the closed-shell Zn^{2+} *ab* initio embedding model potentials (AIMP).[7] The only removed atoms are those connected to the Co^{3+} AIMP from the opposite side of the molecule. The basis sets for all atoms were atomic natural orbitals from the MOLCAS ANO-RCC library. The following contractions are used: [6s5p3d2f1g] for Co, [4s3p2d] for C, N and O, and [2s] for H. The spin-orbit coupling is calculated by the RASSI program.

Structure and characterization data.

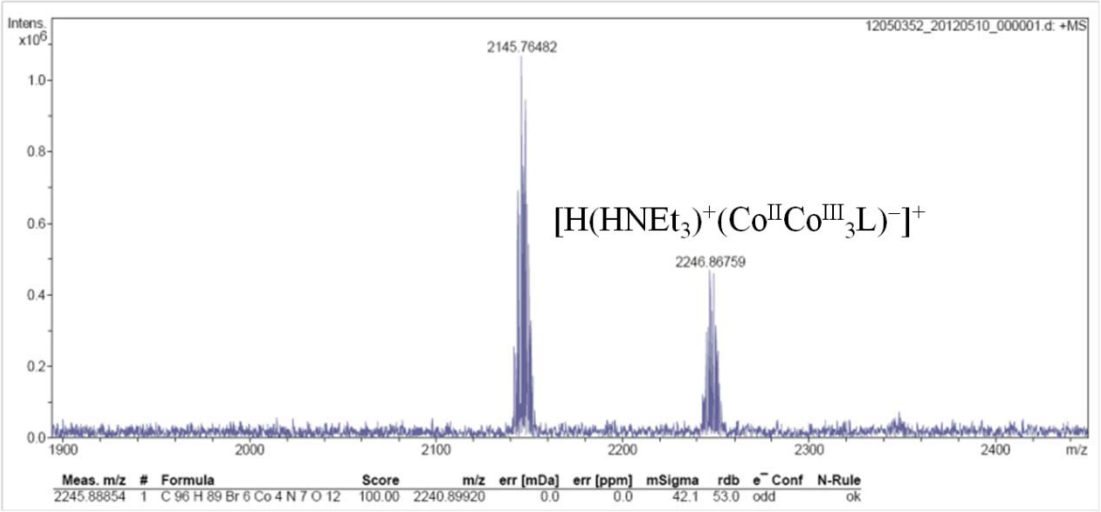

Figure S1. The ESI-MS spectrum of **1** by cation mode.

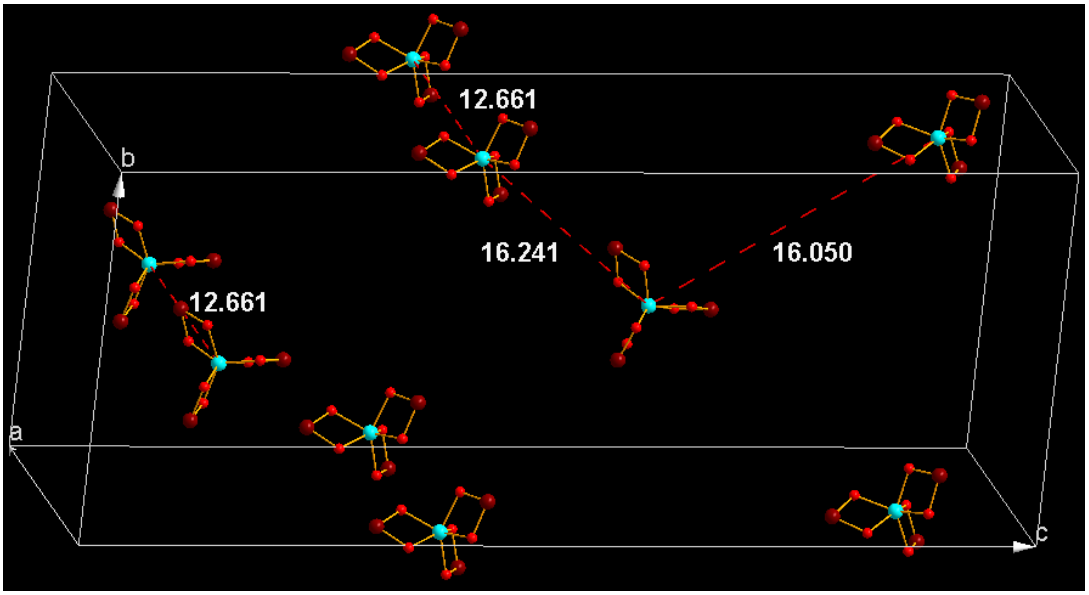

Figure S2. The molecular packing of **1** in a crystal cell, which demonstrates the arrangements of anisotropic axis of Co(II) are in different orientations. The shortest distance of paramagnetic Co(II) ions between neighbor clusters are 12.661 Å. The ligands are omitted for clarity.

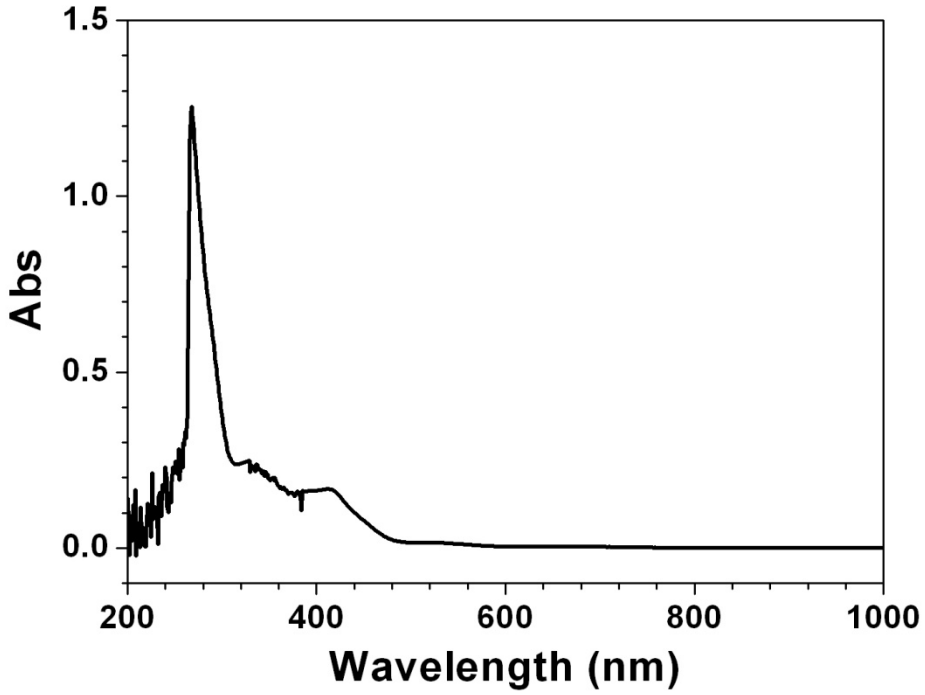

Figure S3. UV-vis absorption spectrum of **1** (10^{-5} M) from 200 to 1000 nm at 298 K.

The magnetic data of compound 1.

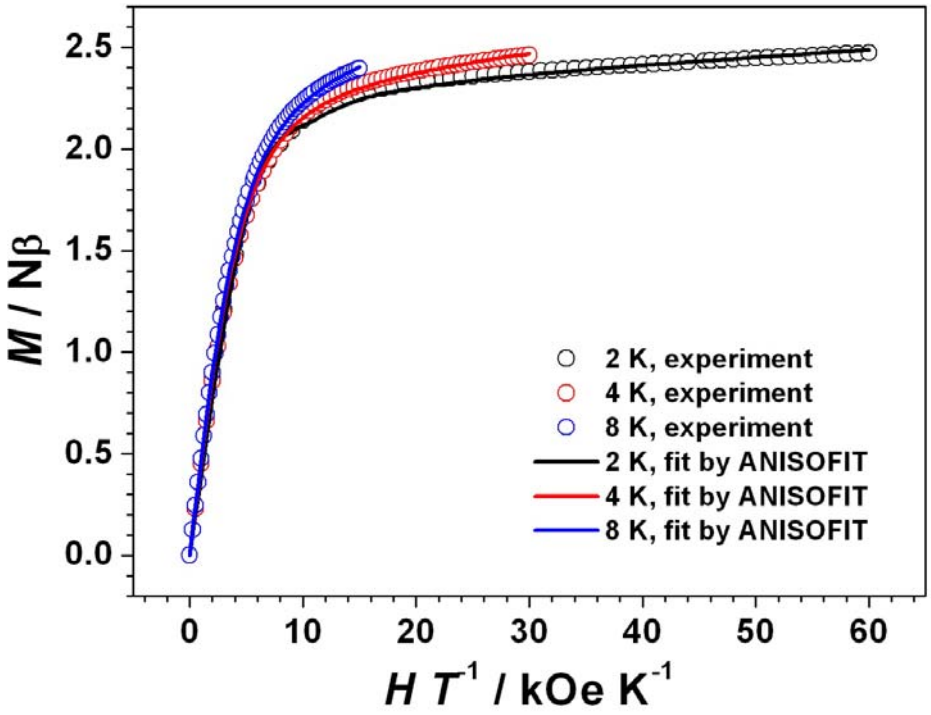

Figure S4. Dc magnetic susceptibility of **1** measured at different temperatures (2 K, 4 K, and 8 K) up to 12 T (hollow point) in PPMS-16 and fitting result using ANISOFIT 2.0 program (solid line).

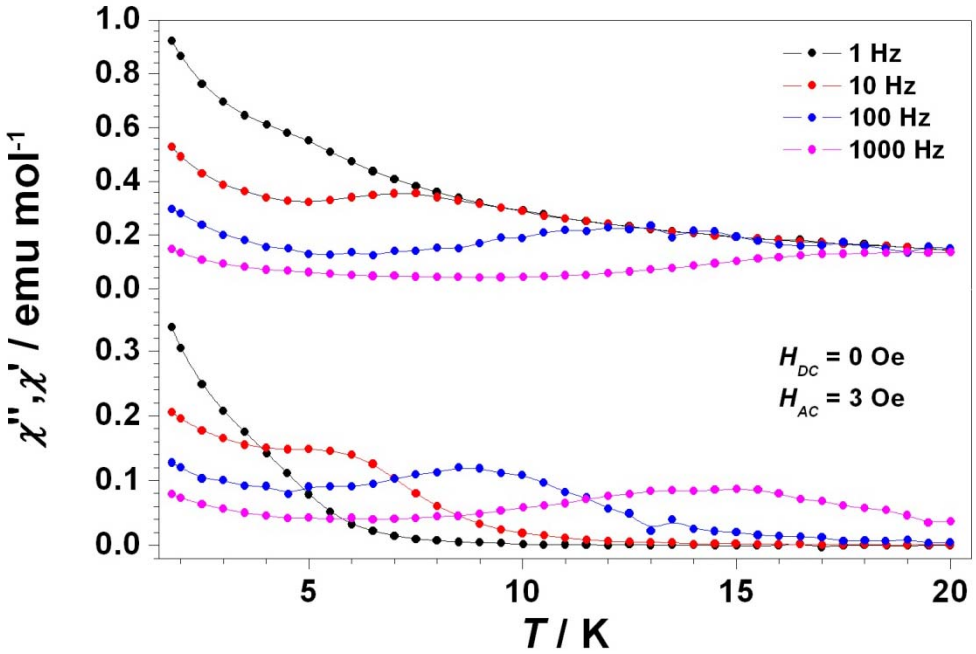

Figure S5. The temperature dependence of ac susceptibility under zero dc field at frequencies from 1 to 1000 Hz for **1** in MPMS.

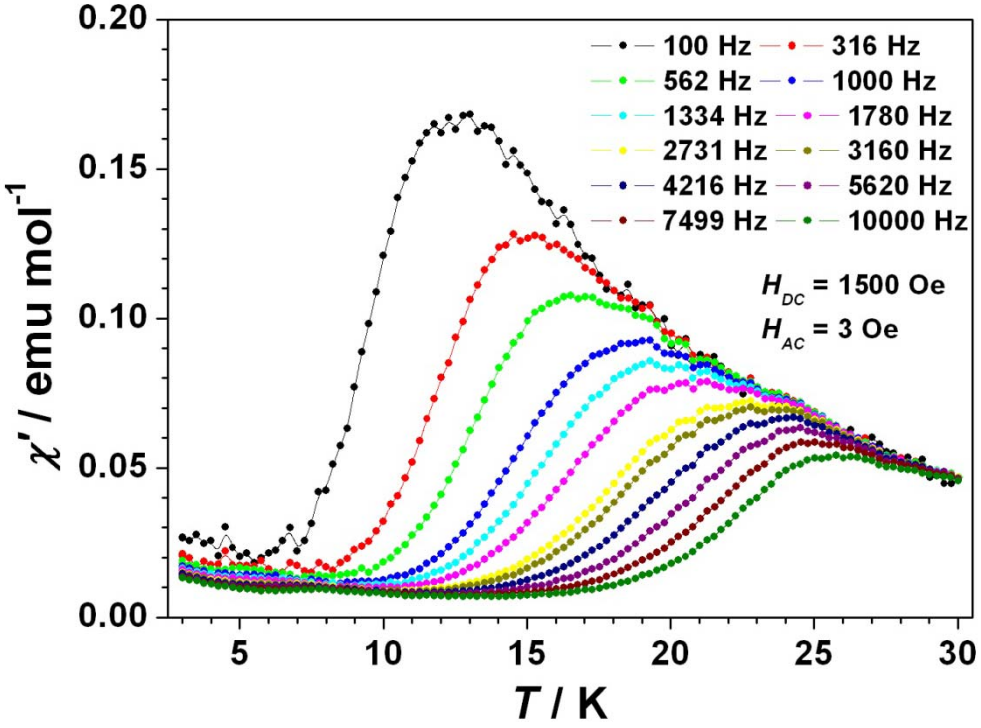

Figure S6. χ' (in-phase) against temperature for **1** under 1500 Oe dc field range from 3 to 30 K in PPMS.

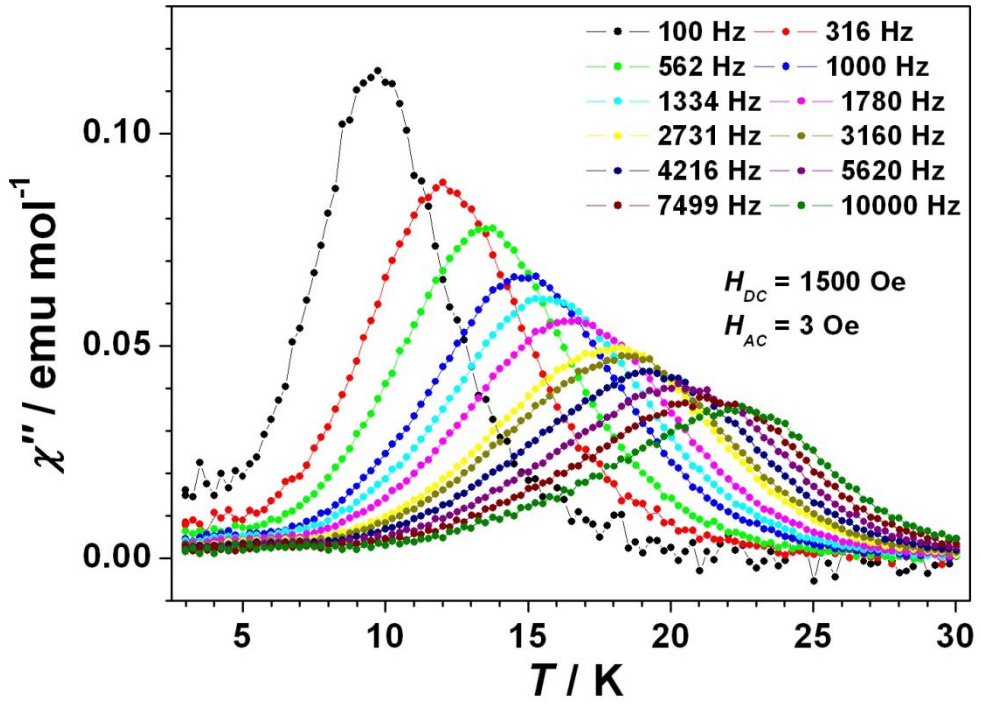

Figure S7. χ'' (in-phase) against temperature for **1** under 1500 Oe dc field range from 3 to 30 K in PPMS.

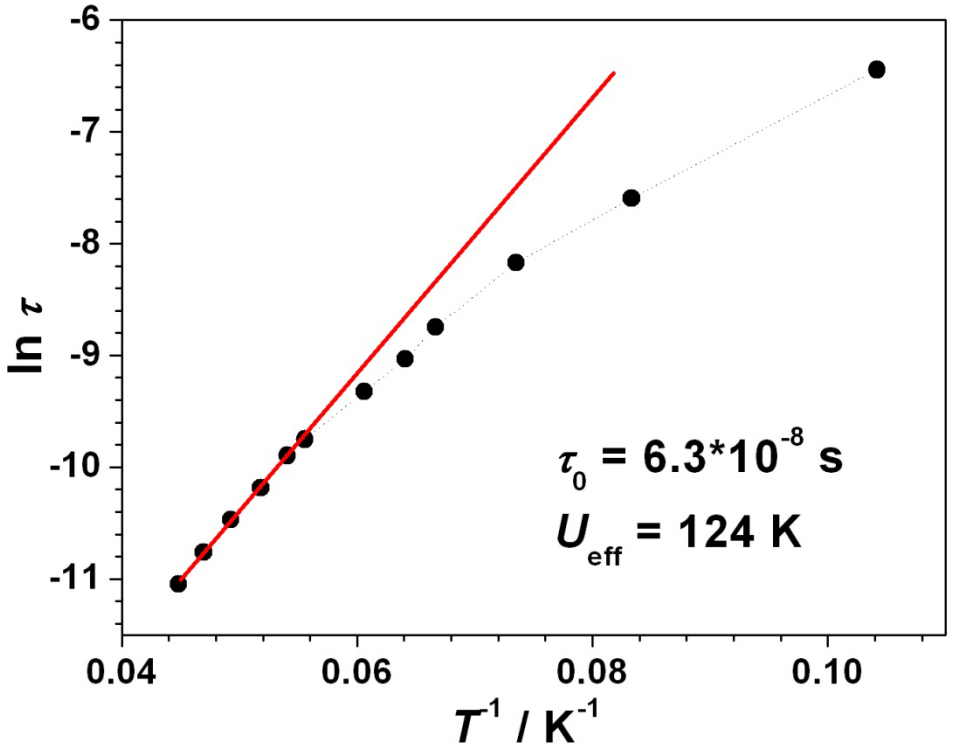

Figure S8. Arrhenius plots of relaxation times of **1** under 1500 Oe dc field, the data was collected from the peaks of χ'' (out-of-phase) against temperature at different frequency.

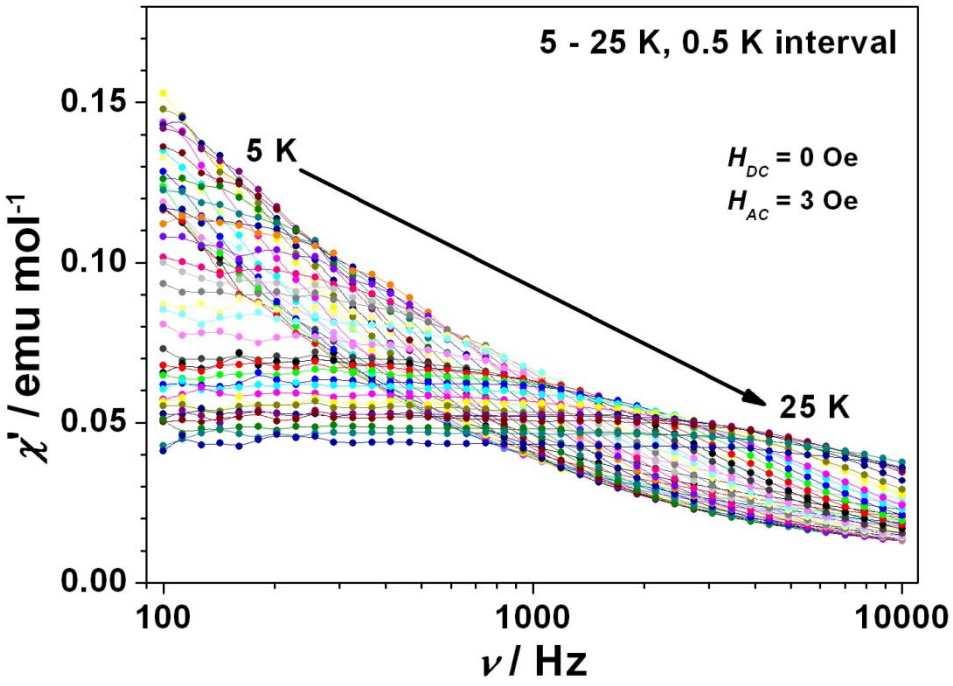

Figure S9. χ' (in-phase) against frequency of **1** under zero dc field range from 100 to 10000 Hz at different temperature (5 to 25 K, 0.5 K interval) in PPMS.

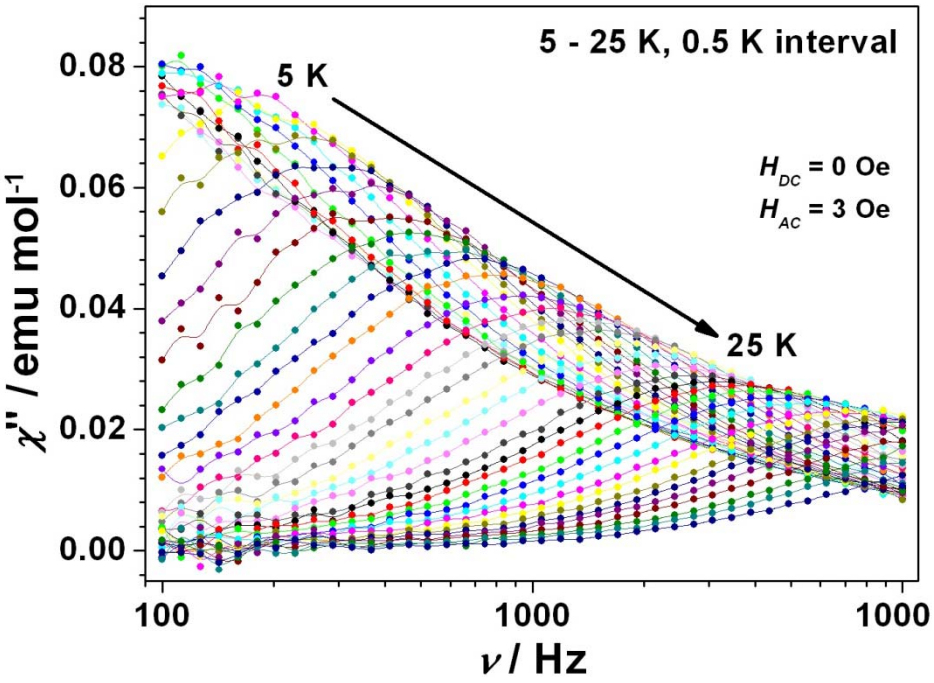

Figure S10. χ'' (in-phase) against frequency of **1** under zero dc field range from 100 to 10000 Hz at different temperature (5 to 25 K, 0.5 K interval) in PPMS.

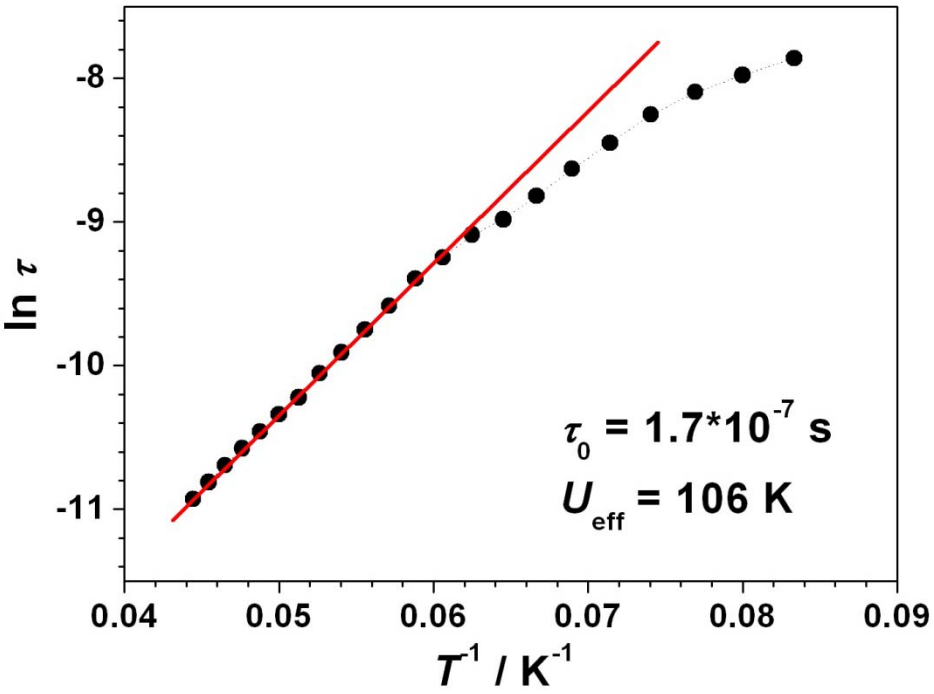

Figure S11. Arrhenius plots of relaxation times of **1** under zero dc field, the data was collected from the peaks of χ'' (out-of-phase) against frequency at different temperature.

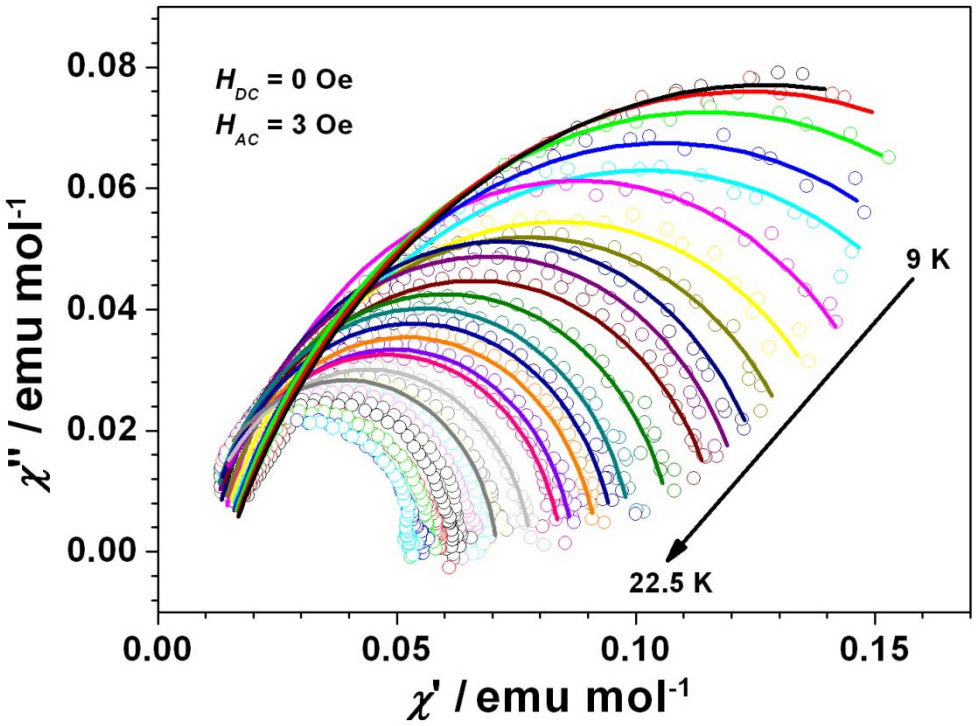

Figure S12. Cole-Cole diagram of **1** under zero applied dc field (ac frequencies range from 100 to 10000 Hz).

Table S3. The parameters of Cole-Cole fitting of **1** under zero applied dc field.

T (K)	X_0	X_t	τ	α	R
9.0	0.01424	0.22616	0.00131	0.19916	2.95×10^{-4}
9.5	0.01405	0.21973	0.00104	0.18947	1.60×10^{-4}
10.0	0.01374	0.20518	0.00085	0.17347	8.22×10^{-4}
10.5	0.01335	0.18981	0.00074	0.16847	9.03×10^{-4}
11.0	0.01253	0.18161	0.00061	0.18460	1.02×10^{-3}
11.5	0.01249	0.15878	0.00043	0.11212	8.08×10^{-4}
12.0	0.01232	0.14945	0.00038	0.14482	8.57×10^{-4}
12.5	0.01127	0.13884	0.00031	0.12944	9.10×10^{-4}
13.0	0.01122	0.12972	0.00027	0.09205	8.76×10^{-4}
13.5	0.01015	0.12431	0.00022	0.09982	5.26×10^{-4}
14.0	0.00975	0.11849	0.00019	0.12290	5.39×10^{-4}
14.5	0.00951	0.10835	0.00015	0.09456	6.49×10^{-4}
15.0	0.00984	0.09960	0.00014	0.07017	8.69×10^{-4}
15.5	0.00952	0.09588	0.00012	0.08639	9.87×10^{-4}
16.0	0.00970	0.09217	0.00010	0.09672	9.04×10^{-4}
16.5	0.00966	0.08718	0.00009	0.09450	8.73×10^{-4}
17.0	0.00909	0.08455	0.00009	0.09332	1.55×10^{-4}
17.5	0.00830	0.07821	0.00007	0.09536	9.71×10^{-4}
18.0	0.00655	0.07102	0.00005	0.08192	9.63×10^{-4}

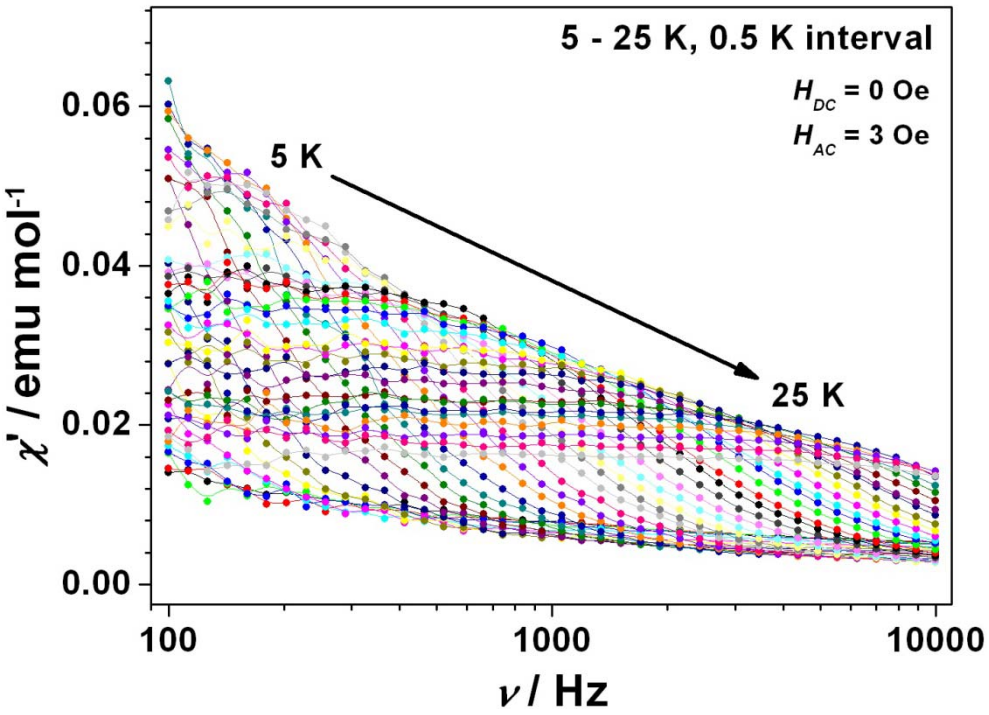

Figure S13. χ' (in-phase) against frequency of **1** under 1500 Oe dc field from 100 to 10000 Hz at different temperatures (5 to 25 K, 0.5 K interval) in PPMS.

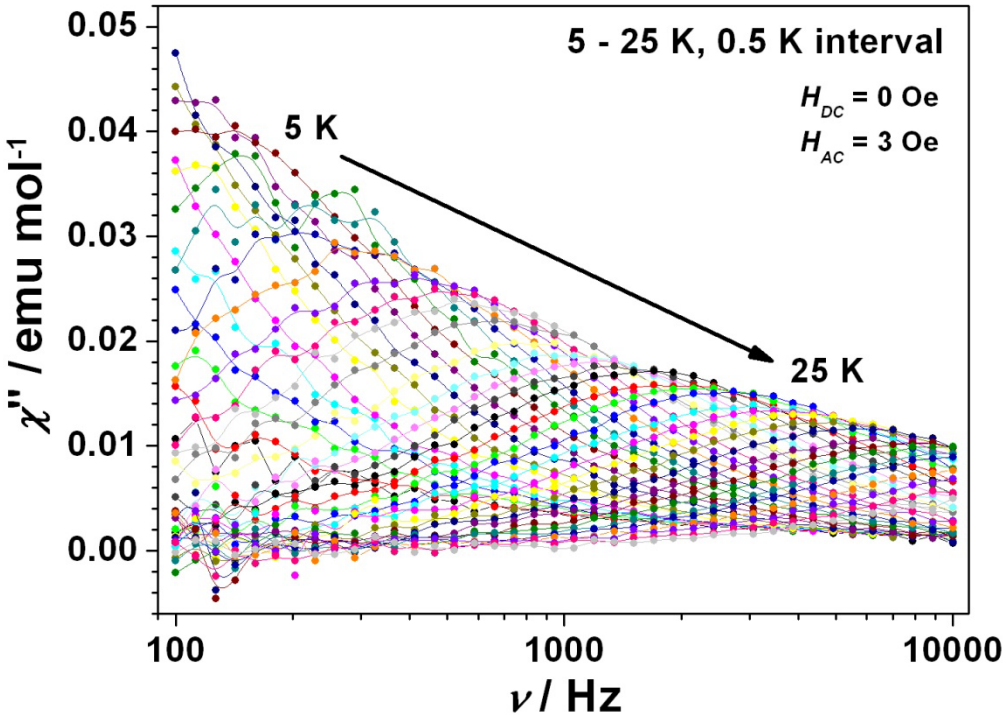

Figure S14. χ'' (out-of-phase) against frequency of **1** under 1500 Oe dc field from 100 to 10000 Hz at different temperatures (5 to 25 K, 0.5 K interval) in PPMS.

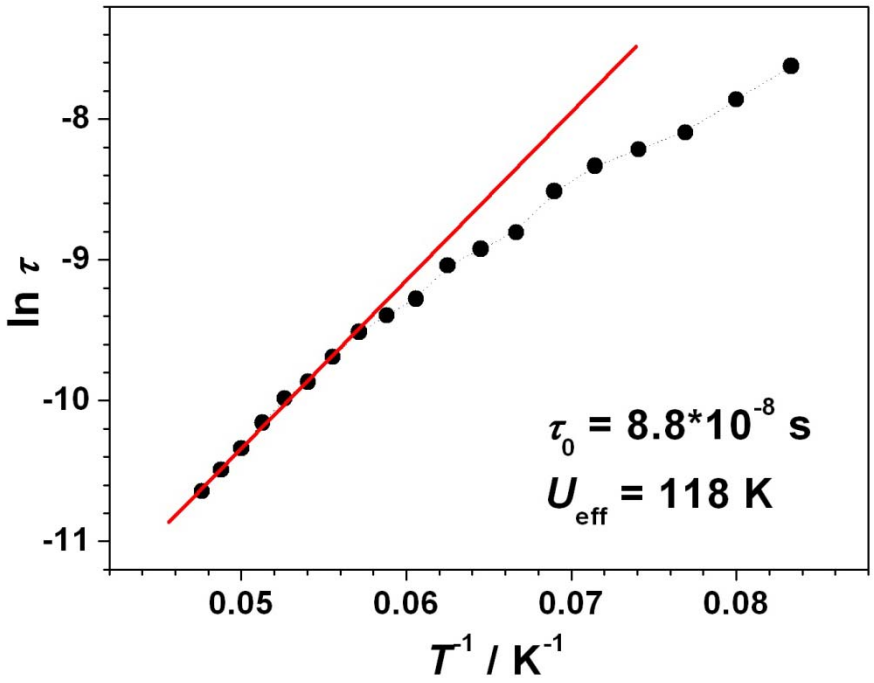

Figure S15. Arrhenius plots of relaxation times of **1** under 1500 Oe dc field, the data was collected from the peaks of χ'' (out-of-phase) against frequency at different temperature.

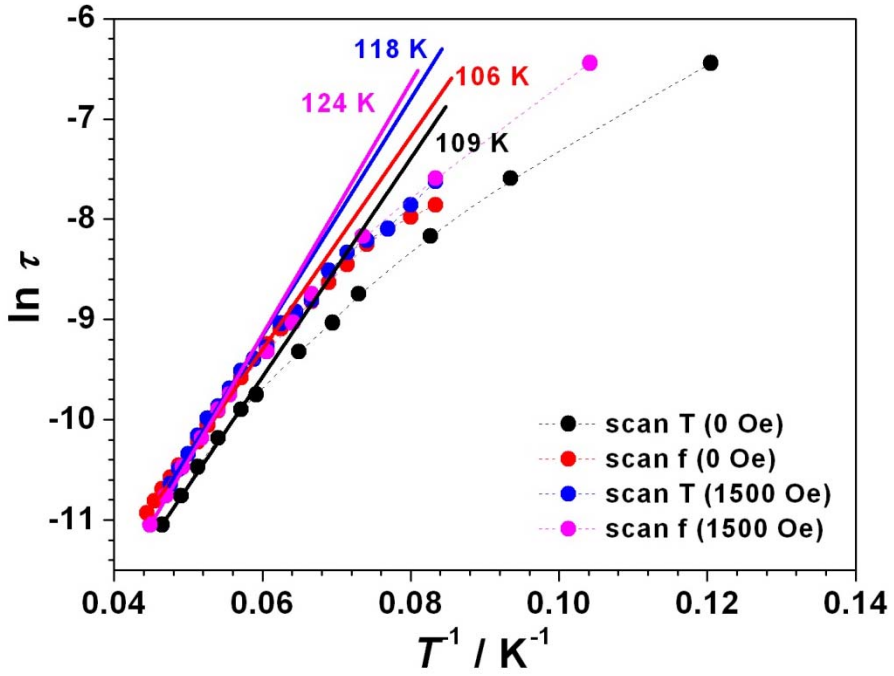

Figure S16. The merge of Arrhenius plots of relaxation times of **1** under different measured conditions, (a) scan temperatures under zero dc field; (b) scan frequencies under zero dc field; (c) scan temperatures under 1500 Oe dc field; and (d) scan frequencies under 1500 dc field.

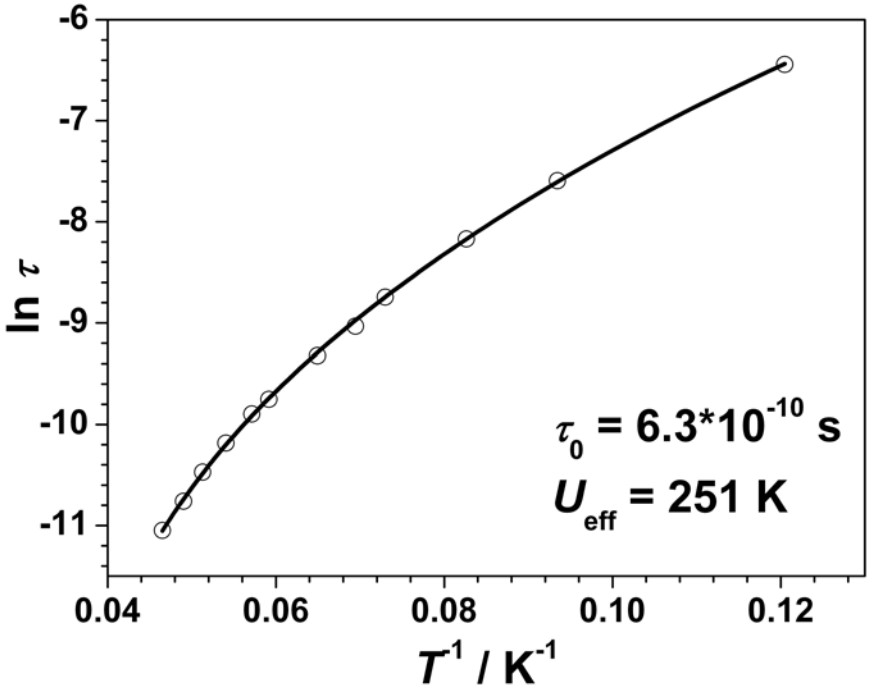

Figure S17. Arrhenius plots of the temperature dependences of relaxation times τ of **1** under zero dc field. Black line represent fit to multiple relaxation processes (containing Raman plus Orbach processes), which has discussed in the below.

The following equation was used to fit the relationship of relaxation time and temperature taking Raman and Orbach processes into account:

$1/\tau = CT^n + \tau_0^{-1} \exp(-U_{eff}/kT)$ $(n \geq 4)$

In this equation, CT^n represents Raman relaxation process and $\tau_0^{-1} \exp(-U_{eff}/kT)$ represents Orbach relaxation process. Many sets of parameters and relaxation time have been tried that heavily correlated with both Raman and Orbach process. The best fits were obtained with n = 4.6, and corresponding C = 0.037, τ_0 = 6.3 × 10^{-10} and U_{eff} = 251 K, which was much higher than the fitted value of 109 K involved only Orbach process. We tried the fitting with n = 4 or 5, but failed to get reasonable results. The newly fitting U_{eff} value of 251 K was consistent with the calculated relaxation barrier (289 K and 311 K) using the spin-Hamiltonian approach and *ab* initio calculations. The results indicated that the Raman Process influenced heavily the Orbach process and reduced dramatically the barrier of slow magnetic relaxation.

The four parameters (C, τ_0, n, and U_{eff}) were fitted only from the limited temperature range that the

out-of-phase ac peaks appeared. At low temperature, the relaxation barrier was also influenced by the QTM process. For the convenience to compare with the reported single TM based SMMs, the relaxation barrier fitted with Arrhenius law was used in the manuscript. The fitting results with both Raman and Orbach process were provided in the SI.

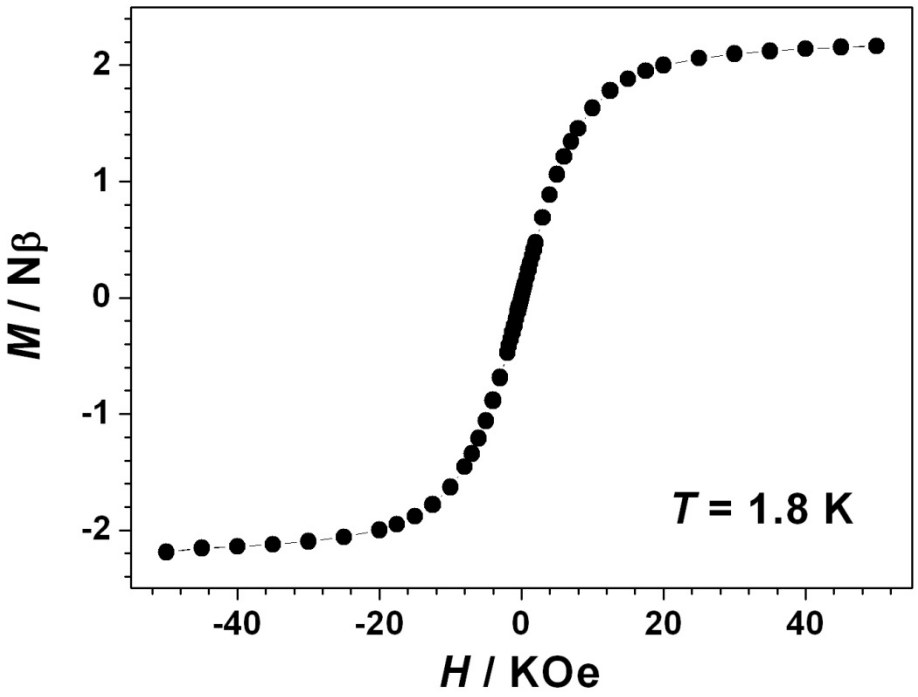

Figure S18. Magnetization versus field measured for the **1** at 1.8 K from -5 T to 5 T in MPMS, no hysteresis loop was observed.

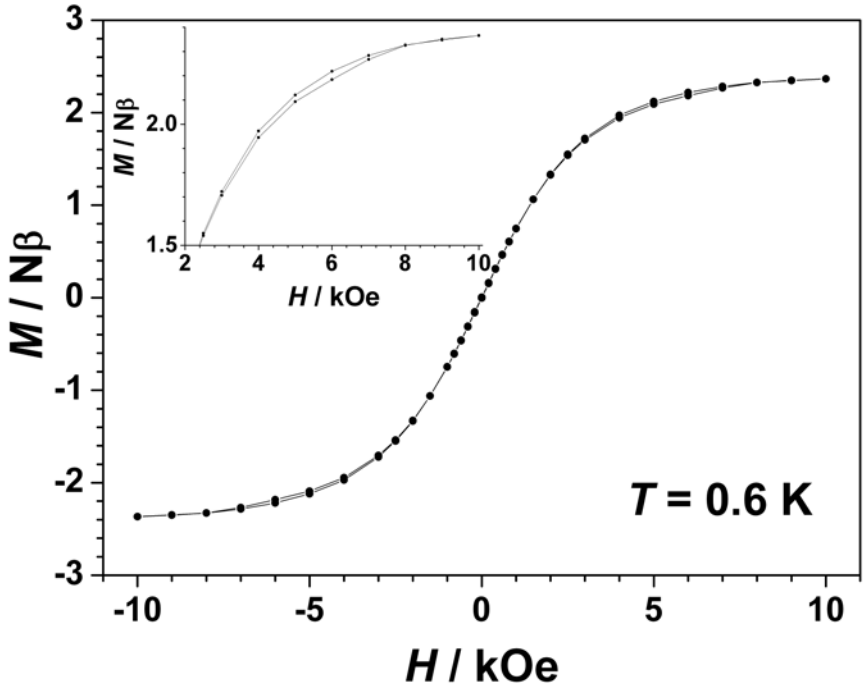

Figure S19. Magnetization versus field measured for the **1** at 0.6 K from -1 T to 1 T in MPMS, small bifurcation was observed.

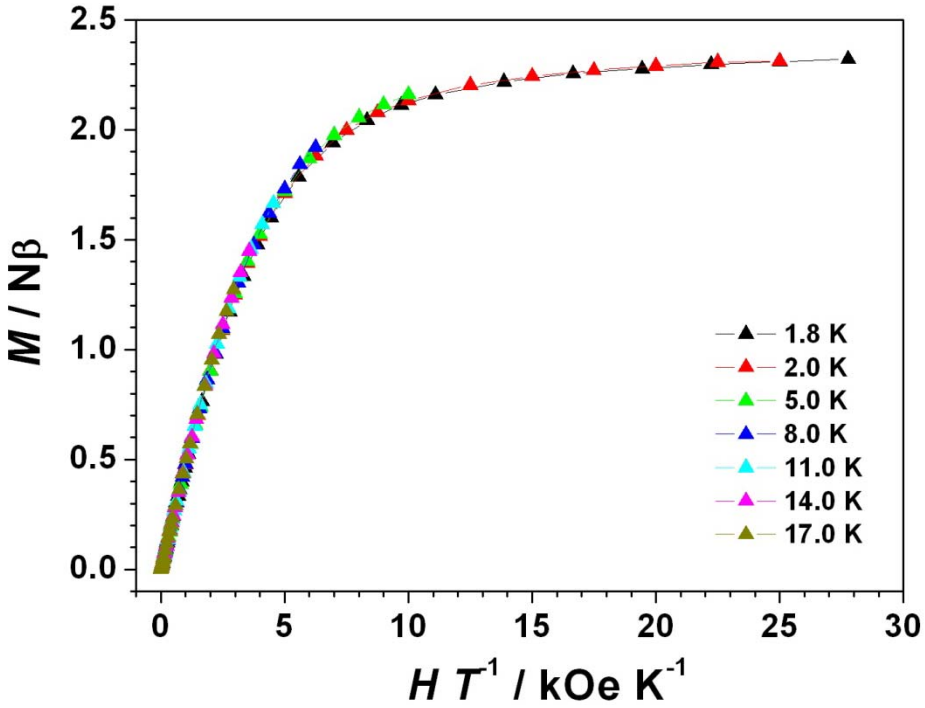

Figure S20. *M vs*. *H*/*T* plots of **1** at different temperatures (1.8 K, 2 K, 5 K, 11 K, 14 K, and 17 K) in MPMS, revealed that the bifurcation of curves were not significant from 0–5 T.

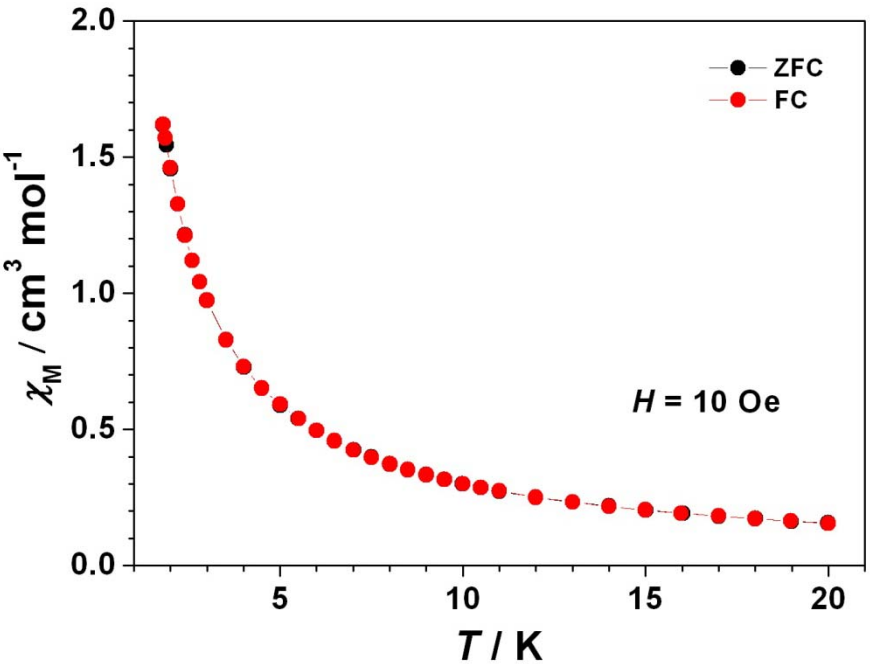

Figure S21. Plots of zero-field cooled magnetization (ZFC) and field-cooled magnetization (FC) of **1** in field of 10 Oe from 1.8 K to 20 K in MPMS, no bifurcation was observed in the measured temperature range.

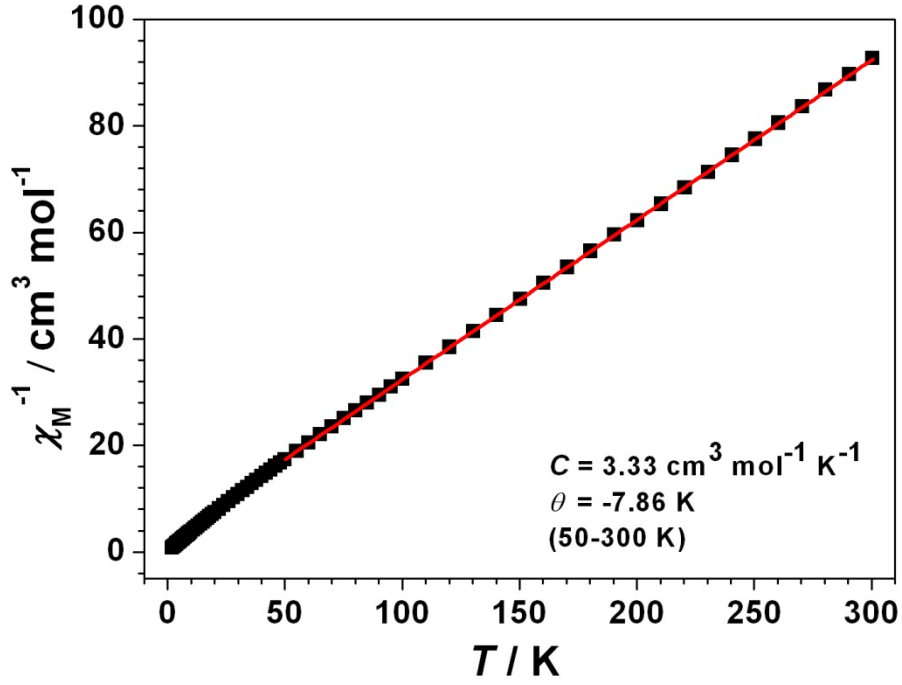

Figure S22. Plots of χ_M^{-1} versus T for **1** under 1 kOe field (The red solid line represents the best fit to the Curie-Weiss expression).

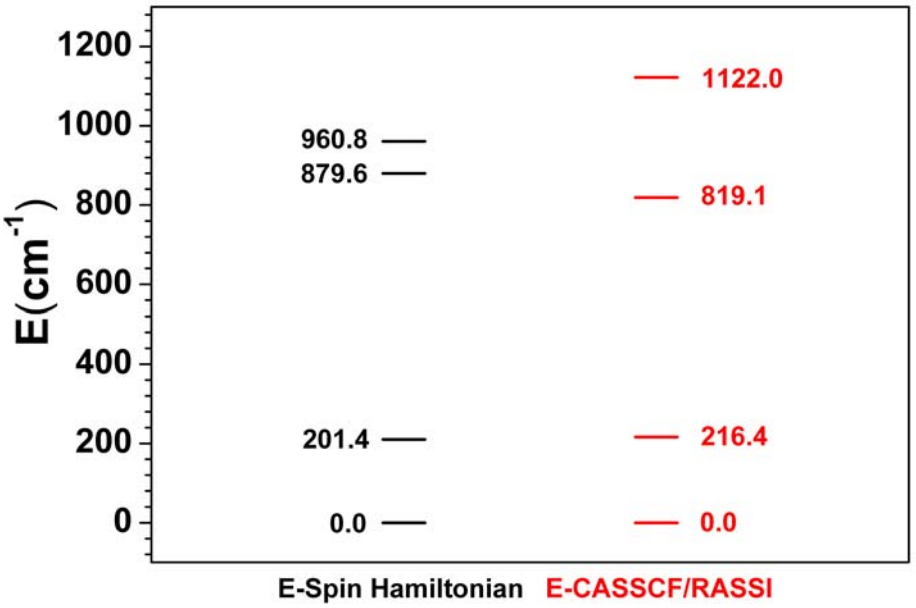

Figure S23. The energy diagram of central Co(II) ion in compound **1** from spin-Hamiltonian approach and *ab* initio calculations.

References

1. G. M. Sheldrick, *SHELXS-97*; University of Gottingen: Gottingen, Germany, 1990.

2. G. M. Sheldrick, *SHELXS-97*; University of Gottingen: Gottingen, Germany, 1997.

3. X.-L. Yu, D. Scheller, O. Rademacher and T. Wolff, *J. Org. Chem.* 2003, **68**, 7386–7399.

4. N. E. Brese and M. O'Keeffe, *Acta Cryst. B* 1991, **47**, 192–197.

5. I.D. Brown, The Chemical Bond in Inorganic Chemistry: The Bond Valence Model. Oxford University Press, 2002.

6. G. Karlstrom, R. Lindh, P. A. Malmqvist, B. O. Roos, U. Ryde, V. Veryazov, P. O. Widmark, M. Cossi, B. Schimmelpfennig, P. Neogrady and L. Seijo, *Comput. Mater. Sci*. 2003, **28**, 222–239.

7. L. Seijo and Z. Barandiarán, *Computational Chemistry*: *Reviews of Current Trends*, 1999, **4**, ed. by J. Leszcynski (World Scientific, Singapur), 55–152.